Nanoscale

Accepted Manuscript

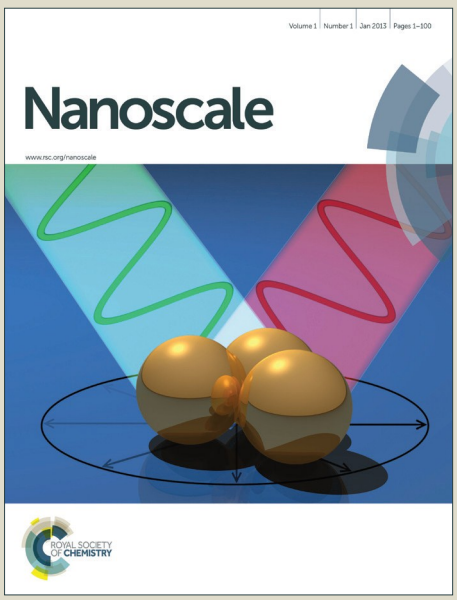

ROYAL SOCIETY OF CHEMISTRY

www.rsc.org/nanoscale

Synergistic Dual-pH Responsive Copolymer Micelles for Impediment of the Blood Drug Release and Motivation of the Intracellular

Hongzhang Deng[1, 3], Xuefei Zhao[1, 3], Jinjian Liu[2], Jianhua Zhang[1], Liandong Deng[1], Jianfeng Liu[2*], Anjie Dong[1, 3*]

[1]Department of Polymer Science and Technology and Key Laboratory of Systems Bioengineering of the Ministry of Education, School of Chemical Engineering and Technology, Tianjin University, Tianjin 300072, China

[2]Tianjin Key Laboratory of Radiation Medicine and Molecular Nuclear Medicine, Institute of Radiation Medicine, Chinese Academy of Medical Science and Peking Union Medical College, Tianjin, 300192, China

[3]Collaborative Innovation Center of Chemical Science and Engineering (Tianjin), Tianjin 300072, China

* Corresponding author. Fax: +86 22 27890707.

** Corresponding author. Fax: +86 22 85683019.

E-mail addresses: ajdong@tju.edu.cn (A. Dong), lewis78@163.com (J. Liu).

Abstract

How to tune the structure of nanocarriers with fast acidic-degradation rate and high stability in physiological condition or during storage is also an intrinsic limitation. In this context, a kind of dual-pH responsive micelles with well-balanced stability, that is, fast hydrolysis in an acidic environment and impediment of the blood drug release with high stability at 7.4 were developed, i.e. the self-assembly micelles of poly(ethylene glycol)-b-(poly ε-caprolactone-g-poly(2,2-dimethyl-1,3-dioxolane-4-yl) methylacrylate-*co*-2 (dimethylamino) ethyl methacrylate) (mPEG-b-(PCL-*g*-P(DA-*co*-DMAEMA))) copolymers with two inert pH responsive moieties of DA and DMAEMA. The fast synergistic acid-triggered disassembly and high stability at physiological condition of the mPEG-b-(PCL-*g*-P(DA-*co*-DMAEMA)) micelles was certificated by ^{1}H-NMR, particle size and optical stability measurements, which was induced and mediated by the synergistic pH responses of the hydrolysis of the ketal in DA moieties and the switch in solubility of tertiary amino moieties (DMAEMA) at mild acid condition. It was observed that the hydrolysis rate of the ketal could be promoted by increasing the contents of DMAEMA moieties. The fast intracellular disassembly of the micelles depending on the contents of DMAEMA moieties was also traced by fluorescence resonance energy transfer (FRET). The *in vitro* release studies showed that the release of DOX from mPEG-b-(PCL-*g*-P(DA-*co*-DMAEMA)) micelles at mild acid condition was significantly accelerated by increasing the contents of DMAEMA moieties, while greatly impeded the drug release in the physiological conditions. The antitumor activity of DOX-loaded micelles was studied in MCF-7 and 4T1 cells *in vitro* and in 4T1 tumor-bearing Balb-c mice *in vivo*. The results indicated the DOX-loaded micelles with higher content of DMAEMA moieties exhibited enhanced anti-cancer activity. Collectively, the synergistic dual-pH responsive design of mPEG-b-(PCL-*g*-P(DA-*co*-DMAEMA)) micelles provided a new operably for improving anticancer drug delivery efficiency.

Keywords: synergistic pH response, protonation, DMAEMA, drug delivery, DOX

1. Introduction

Biodegradable polymeric micelles based on amphiphilic block copolymers for drug delivery with high therapeutic efficacy have emerged as one of the most promising platforms in successful cancer chemotherapy. Polymeric micelles offer the distinct advantages of accumulation at the tumor site *via* the enhanced permeability and retention (EPR) effect [1-5]. However, the EPR effect can only enhance the accumulation of micelles in tumor tissues. The insufficient intracellular drug release from polymeric micelles also limited the dosages of anticancer drugs to a desired therapeutic concentration at the targeting site, hampering the efficacy of cancer chemotherapy [6]. To overcome this challenge, nanocarriers capable of controlled response to physiological events such as changes in extracellular pH are particularly useful in the field of therapeutics and diagnostics[7-11]. However, the intrinsic limitation of nanocarriers on fast degradation under acidic conditions and the higher stability of the polymer at pH 7.4 or during storage were also the main challenges in the drug delivery applications.

To obtain fast degradation micelles under acidic conditions, pH-response bonds such as, hydrazone, cis-acotinyl, and acetal have been introduced to the main chain or side chain to enhance the speed of drug release for tumor-killing efficacy[12-15]. The degradation or hydrolysis rate of a biodegradable polymer was a key factor for polymeric micelles used in biomedical applications to achieve desired therapeutic effects with a lower dose and to minimize undesirable side effects[16]. However, the hydrolysis of those polymers at pH 7.4 was usually also observed[17]. The premature drug release from polymeric micelles before it reaches the target tissue hampers the efficacy of cancer chemotherapy. Therefore, polymers with well-balanced stability, that is, fast degradation in an acidic environment and high stability both at pH 7.4 and during storage, are highly desired for intracellular drug-delivery applications.

In order to obtain safe and stable pH response polymeric micelles, a moderate pH response ketal wiht the good stabilty at physiological environment had been developed extensively

over past several decades for drug vehicles[18]. Despite the advances of good stability at pH 7.4, the existing ketal or acetal-containing polymeric materials can't undergo rapid acid catalyzed hydrolysis in acidic pH (pH 6~5) unless fully hydrated, which may in some instances reduce the drug delivery efficacy[19-23]. Therefore, it appears to be impossible using a single pH response moiety to construct the ideal polymers that are stable both at storage and at pH 7.4, while quickly degrade under mildly acidic conditions[24].

In this study, synergistic dual-pH response poly(ethylene glycol)-b-(poly ε-caprolactone-*g*-poly((2,2-dimethyl-1,3-dioxolane-4-yl methyl acrylate)-*co*-2 (dimethylamino) ethyl methacrylate), mPEG-b-(PCL-*g*-P(DA-*co*-DMAEMA)) was developed by incorporating tertiary amino groups of DMAEMA into pH-response ketal groups of DA. mPEG-b-(PCL-g-P(DA-*co*-DMAEMA)) presents well-balanced stability, that is, fast hydrolysis in an acidic environment and impediment of the blood drug release with high stability at pH 7.4. As shown in Scheme 1, an efficient approach was developed with modulating the inert pH hydrolysis of the ketal (DA) by incorporating amount of tertiary amino groups moieties (DMAEMA), which are highly stable under neutral conditions but fast switch to hydrophilic by pH triggered protonation in acid environment[25-30]. The protonation of DMAEMA leaded to comformational change of P(DA-*co*-DMAEMA) from crimp to extend and intense mutual exclusion in the core of PCL-P(DMAEMA-*co*-DA), resulting an increase in water uptake, enhancing the solubility in water and activate the ketal hydrolysis. Therefore, fast disassembly of the mPEG-b-(PCL-*g*-P(DA-*co*-DMAEMA)) micelles at acid environment and high stability at pH 7.4 was induced and mediated by the synergistic dual-pH responses of the hydrolysis of the ketal in DA moieties and the switch in solubility of tertiary amino moieties (DMAEMA). The results of ^{1}H-NMR, particle size and optical stability measurements shown that the hydrolysis rate of the ketal of DA moieties could be greatly promoted by increasing the contents of DMAEMA moieties at acid environment. Meantime, the *in vitro* release studies indicated that the mPEG-b-(PCL-*g*-P(DA-*co*-DMAEMA)) micelles containg a series

of contents of DMAMEA moieties in DA moieties kept high stability at pH 7.4. What's more, *in vivo* efficacy of such system was also evaluated. These results are helpful for designing synergistic dual-pH-sensitive polymers that may have potential application for intracellular anticancer drug delivery.

2. Materials and mehtods

2.1. Materials.

mPEG-b-P(CL-*co*-BMPCL) and (2,2-dimeth yl-1,3-dioxolane-4-yl) methyl acrylate (DA) were synthesized as reported[4, 31] and detail information was given in supporting information. The structure of DA was confirmed by ^{1}H-NMR (Fig. S1). ε-caprolactone (CL) purchased from Sigma-Aldrich was dried over calcium hydride for 48 h at room temperature and distilled under reduced pressure just before used. Methoxy poly (ethylene glycol) (mPEG, M_n = 5.0×10^3 g/mol), stannous octoate ($Sn(Oct)_2$), copper(I) bromide (Cu(I)Br) 1,2-Isopropylideneglycerol and 2-(dimethylamino)-ethylmethacrylate (DMAEMA) were purchased form GL Biochem (Shanghai) Ltd.. Methylene dichloride (DCM) were refluxed over CaH_2 and distilled prior to use. Dimethyl sulfoxide (DMSO) were dried over CaH_2 and distilled under reduced pressure before use. Doxorubicin hydrochloride (DOX·HCl) was purchased from Wuhan Hezhong Biochemical in manufacturing co.,Ltd (China, Wuhan). All other regents were analytical grade and used as received.

The deuterated phosphate buffers (PB) with different pHs were prepared from NaOD (40% in D_2O) and deuterated phosphoric acid (85% in D_2O) by changing their ratios.

Dulbecco's modified Eagle's medium (DMEM), Opti-MEM and bovine serum (FBS) were purchased from Invitrogen Corporation (Carlsbad, CA). Dimethyl sulfoxide (DMSO), 3-[4,5-dimethylthiazol-2-yl]-2,5-diphenyltetrazolium bromide (MTT), 1,1-dioctadecyl-3,3,3,3-tetramethylindocarbocyanine perchlorate (DiI), and 3,3-dioctadecyloxacarbocyanine, perchlorate (DiO) were purchased from Sigma-Aldrich.

2.2. Characterization

^{1}H-NMR spectra were recorded on a Varian Inova 500 spectrometer operating at 500 MHz (Varian Inc., Palo Alto, USA) using $CDCl_3$ as a solvent and tetramethylsilane (TMS) as the internal standard. The number-average molecular weight (M_n) and polydispersity index (M_w/M_n) of copolymers were determined by gel permeation chromatography (GPC) using a Malvern Viscotek GPC max system which was equipped with a porous styrene divinylbenzene copolymer-based column (CLM3009, T6000M, General Mixed, Org 300 × 7.8 mm). THF was used as the eluting solvent with a flow rate of 1 mL/min and polystyrene was used as standard for calibraten. The size and size distribution (PDI) of micelles were performed using a laser particle size analyzer (zetasizer Nano, Malvern, UK) at a wavelength of 633 nm with a constant angle of 173 ^{o}C. The diameter of micelles was received from the average of three measurement results. Morphologies of micelles were observed under a Hitachi H600 transmission electron microscopy (TEM) system at operated voltage of 75 kV. For TEM measurement, the sample was prepared by adding a drop of micelles solution onto the copper grid, and then the sample was air-dried and measured at room temperature.

2.3. Synthesis of mPEG-b-(PCL-*g*-P(DA-*co*-DMAEMA)).

mPEG-b-(PCL-*g*-P(DA-*co*-DMAEMA)) was synthesized by atom transfer radical polymerization (ATRP) of DA and DMAEMA using mPEG-b-P(CL-*co*-BMPCL) as marcroinitiator. mPEG-b-P(CL-*co*-BMPCL) (1.37 g, 0.1 mmol), CuBr (0.0429 g, 0.3 mmol), and bPy (0.0936 g, 0.6 mmol) were added into Schlenk tube under nitrogen. DA (0.2556 g, 1.8 mmol) and DMAEMA (0.2556 g, 1.8 mmol) were also injected into this reactor. The mixture was degassed by three vacuum/nitrogen cycles to remove the oxygen of reaction system. The bulk polymerization was carried out at 65 ^{o}C for 14 h and then the product was dialyzed (M_n = 3500) against water for 24 h to remove residual copper species and unreacted monomers and then freeze-dried to obtain mPEG-b-(PCL-*g*-P(DA-*co*-DMAEMA)). The final yields were over 85%.

2.4. Micelles formation and critical micelle concentration (CMC).

mPEG-b-(PCL-*g*-P(DA-*co*-DMAEMA)) micelles were prepared by dialysis method. Typically, mPEG-b-(PCL-*g*-P(DA-*co*-DMAEMA)) was dissolved in dimethylformamide (DMF) and added dropwise to double distilled water. After that, the solution was transferred to a 3500 Da molecular weight cutoff dialysis bag and dialyzed to remove the organic solvents.

The CMC was measured by a steady state fluorescent-probe methodology using pyrene as probe on a Varian fluorescence spectrophotometer at room temperature [32]. The pyrene-loaded micelles were diluted with the concentration between 10^{-6} and 0.1 mol/L in deionized water. The final pyrene concentration in the copolymer solution was kept at 6×10^{-7} mol/L. The solution was shaken vigorously and then allowed to equilibrate at 25 ^{o}C for at least 24 h. The pyrene excitation spectra with different copolymer concentrations were measured at the detection emission wavelength (λ_{em}=373 nm). The CMC value was evaluated from the intersection of the tangent to the horizontal line of I_{337}/I_{333} with relative constant value and the diagonal line with rapidly increased I_{337}/I_{333} rate.

2.5. pH dependent stability monitored by an optical analyzer turbiscan.

The pH dependent stability assay was performed using an optical analyzer Turbiscan (Formulaction, France) [33, 34]. The mPEG-b-(PCL-*g*-P(DA-*co*-DMAEMA)) micelles (20 mL, 5 mg/mL) were allocated in a cylindrical glass tube and measurements were carried out using a pulsed near infrared LED source at a wavelength of 880 nm. The light which was transmitted (T) and backscattered (BS) through the whole height of sample was recorded. A latex suspension and silicon oil were used as reference standards and spectroscopic records were computed as percentage with respect to these standards. The variation of the droplet volume fraction (migraten) size (coalescence) were observed as both a variation of backscattering (△ BS) and light transmission (△T) profiles. The samples were scanned every 1 hour of 12 hours. The Turbiscan Easysoft Converter software was used for data elaboraten. Experiments were carried at the room temperature.

2.6. Preparaten of drug-loaded micelles.

Typically, mPEG-b-(PCL-*g*-P(DA-*co*-DMAEMA)) and DOX were dissolved in DMF, the mixture solution was dropwise added to double distilled water under magnetic stirring. The mixture was placed in a dialysis bag (M_n = 3500 Da) and free dialyzed against a phosphate buffer (pH 7.4) to form micelles. The amount of DOX was determined by UV-Vis spectrophotometer. Drug loading content (DLC) and drug loading efficiency (DLE) were calculated from the following equations:

$$\text{DLC}\,(\%) = \frac{\text{weight of loaded drug}}{\text{weight of drug - loaded micelles}} \times 100\% \quad \text{-------}[1]$$

$$\text{DLE}(\%) = \frac{\text{weight of loaded drug}}{\text{weight of drug in feed}} \times 100\% \quad \text{-------}[2]$$

2.7. In vitro release of DOX.

In vitro release profiles of DOX from mPEG-b-(PCL-*g*-P(DA-*co*-DMAEMA)) micelles were investigated in different media, i.e. acetate buffer (10 mM, pH 5.0), phosphate buffered solution (PBS) (10 mM, pH 6.5), and PBS (10 mM, pH 7.4) To obtain drug release profile, 5 mL DOX-loaded mPEG-b-(PCL-*g*-P(DA-*co*-DMAEMA)) micelles (1 mg/mL) were sealed in a dialysis tube (M_n = 3500 Da) and incubated in 25mL release media. The cumulative drug release percentage was calculated by the following equation:

$$Er\ (\%) = \frac{V_e \sum_{1}^{n-1} C_i + V_0 C_n}{m_{DOX}} \times 100\% \text{-------}[3]$$

Where m_{DOX} represents the amount of DOX in the micelles, V_0 is the whole volume of the release media (V_0 = 25 mL), V_e is the volume of the replaced media (V_e = 5 mL), and C_n represents the concentration of DOX in the sample.

2.8. MTT assay.

The biocompatibility of micelles assessed with a methyl tetrazolium (MTT) viability assay against MCF-7 cells and 4T1 cells as described previously. The cells were plated in a 96-well plate (5×10^3 cells/well) using DMEM medium supplemented with 10% fetal bovine serum

(FBS), 1% L-glutamine, antibiotics penicillin(100 IU/mL) and streptomycin(100 μg/mL) for 1 day. The medium was aspirated and replaced by 80μL of fresh medium supplemented with 10% FBS. A total of 20 μL of mPEG-b-(PCL-*g*-P(DA-*co*-DMAEMA)) micelles in PBS (10 mM, pH 7.4) was added to yield final micelle concentrations. The cells were cultured at 37 ºC in an atmosphere containing 5% CO_2 for 1 day. The medium was aspirated and replaced by 100 μL of fresh medium. A total of 10 μL of MTT solution (5 mg/mL) was added. The cells were incubated for another 4 h. The medium was aspirated, the MTT-formazan generated by live cells was dissolved in 200 μL of DMSO, and the absorbance at wavelength of 570 nm of each well was measured using a microplate reader. The relative cell viability (%) was determined by comparing the absorbance at 570 nm with control, which contained only culture medium. Data are presented as average ±SD (n = 3).

2.9. Cell uptake studies.

Intracellular release of DOX from DOX-loaded mPEG-b-(PCL-*g*-P(DA-*co*-DMAEMA)) micelles was followed with confocal laser scanning microscopy (CLSM, Leica AF 6500, Leica Microsystems Germany) using MCF-7 cells. The cells were cultured on microscope slides in a six well plate (5×10^5 cells/well) using DMEM medium supplemented with 10% FBS, 1% L-glutamine, antibiotics penicillin(100 IU/mL), and streptomycin (100 μg/mL). The cells were incubated with DOX-loaded micelles or free DOX for 4 or 24 h at 37 ºC in a humidified 5 % CO_2-containing atmosphere. The culture medium was removed and the cells were rinsed three times with PBS. Meanwhile, Lysotracker Green DND-26 (Invitrogen, Carlsbad, CA) was used to indicate the endosome/lysosome organelles, and Hoechst 33342 was used to stain cell nuclei. Imaging processing programs were coded in Interactive Data Language.

2.10. Endocytosis inhibition experiments

Cells were seeded at a density of 10^5 cells/well in the 6-well plates. After 24 h incubation in complete medium, cells were incubated with different inhibitors in serum-free medium for 1 h.

Next, the medium was replaced with complete medium containing mPEG-b-(PCL-*g*-P(DA-*co*-DMAEMA)) respectively at doxorubicin concentrations of 10 μg/ml and the same inhibitors for another 1 h[35].

The control group was incubated in serum-free medium without inhibitors before the addition of mPEG-b-(PCL-*g*-P(DA-*co*-DMAEMA)). Measurements for each group were repeated three times. After treatment, all the samples were collected and tested by flow cytometry. To evaluate the energy dependent pathway, the cells were pretreated in serum-free medium at 4°C for 1 h. After that, cells were incubated in complete medium containing mPEG-b-(PCL-*g*-P(DA-*co*-DMAEMA)) at 4°C for 1 h. Another method was used to decrease the production of ATP by adding 10mM NaN3. Other inhibitors were added at the following final concentrations: chlorpromazine hydrochloride 10μg/ml, dynasore 80 μM, methyl-β-cyclodextrine (MβCD) 10 mM, nystatin 5 mg/ml.

2.11. *In vivo* tumor inhibition study

BALB/c mice (male, 4–6-weeks-old) were purchased from Vital River Laboratories (Beijing, China). All animal procedures were performed according to the guidelines of Administration of Experimental Animals (Tianjin, revised in June 2004). 4T1 tumor-bearing balb-c mice were used to assay the therapeutic efficacy of DOX-loaded micelles. The mice were randomized divided into four groups (n = 10 per group) and treated with normal saline (as control group), DOX-loaded mPEG-b-(PCL-g-PDA_{30}), DOX-loaded mPEG-b-(PCL-g-P(DA_{30}-*co*-$DMAEMA_{20}$)) micelles or free DOX (DOX 5 mg/kg). Each sample was intravenously injected via vein on days 0, 2, 4, 6, 8, and 10. Tumor growth was measured every other day and the tumor volume was calculated by the formula: tumor volume (mm^3) = (length × $width^2$) × 1/2. Additionally, the body weight and survival rate of mice in each group were also monitored for one month.

2.12. Histomorphological Analysis.

Tissues were examined for histopathology after staining with hematoxylin and eosin (H&E). Tumor, liver, spleen and kidney were collected and fixed for 24 h in 4% paraformaldehyde, then tissue samples were trimmed, embedded in paraffin, and cut into 8-μm-thick sections for H&E assays according to the standard staining protocol. The photos were taken using optical microscope (Leica DMI6000 B).

2.13. Statistical Analysis.

All statistical analysis was performed using SPSS 16.5 software. The statistical significance of differences was determined by one-way analysis of variance (ANOVA). All statistical tests were two-sided, and *$p < 0.05$ and **$p < 0.001$ were used in this study to show statistical significance. The results are shown as mean ± standard deviation.

3. Results and discussion

3.1. Synthesis and Characterization of mPEG-b-(PCL-*g*-P(DA-*co*-DMAEMA)).

As shown in Scheme 2, mPEG-b-(PCL-*g*-P(DA-*co*-DMAEMA)) was obtained in one step, that is, ATRP of DA and DMAEMA. Through ATRP, DA and DMAEMA was grafted from PCL chain to get mPEG-*b*-(PCL-*g*-P(DA-*co*-DMAEMA)) and all characteristic signals could be clearly seen in Fig. 1B. (r at 0.8 ppm for the -C$\underline{H}_3$ in DA blocks and t at 2.68 for the -C$\underline{H}_2$- in the DMAEMA). The characteristic peak of -C$\underline{H}$- in the DA unit was at 4.29. The characteristic peak of -C$\underline{H}_3$ in the DMAEMA unit was at 2.30 ppm. The integral of signal at 2.68 ppm (-C$\underline{H}_2$-) and 4.29 ppm (-CH-) was used for determining the numbers of DMEAMA and DA in the polymer and the results are summarized in Table 1. Gel permeation chromatography (GPC) results showed that these copolymers had unimodal distributions with moderate polydispersity index (PDI) of 1.1 - 1.3 and molecular weights were in parallel with those determined by ^{1}H-NMR (Table 1).

3.2. Preparation and characterization of micelles.

mPEG-b-(PCL-*g*-P(DA-*co*-DMAEMA)) micelles were prepared by solvent exchange method. Laser particle size analyzer measurements showed that mPEG-b-(PCL-*g*-P(DA-*co*-

DMAEMA)) formed monodisperse micelles with low PDI of about 0.2 and sizes of about 100 nm (Table 2). The size of different structure of mPEG-b-(PCL-*g*-P(DA-*co*-DMAEMA)) polymers was investigated as shown in the Fig. 2. The detaile information was summarized in Table 2. Laser particle size analyzer measurements showed that mPEG-b-(PCL-*g*-P(DA-*co*-DMAEMA)) yielded micelles with an average size ranging from 92 to 143 nm and a low polydispersity index (PDI < 0.2). The size of mPEG-b-(PCL-*g*-P(DA-*co*-DMAEMA)) micelles were higher than that of mPEG-b-(PCL-*g*-PDA). Moreover, the diameter of mPEG-b-(PCL-*g*-P(DA-*co*-DMAEMA)) micelles increased with the increase of DMAEMA units. The results can be ascribed to that the introduction of DMAEMA groups decreased the crystalization of PCL segment and created a steric barrier around PCL core, thus leading to forming looser and larger aggregates. TEM was also used to observe the morphology of mPEG-b-(PCL-*g*-P(DA-*co*-DMAEMA)) micelles, which revealed that mPEG-b-(PCL-*g*-P(DA-*co*-DMAEMA)) can form stable micelles with a well-defined spherical shape and a homogeneous size distribution around 100 ~ 130 nm depending on composition. Moreover, the increase of particle size of micelles with increasing DMAEMA content was also observed, which was consistent with the laser particle size analyzer results. Compared with the size determined by dynamic light scattering, the smaller sizes observed by TEM observations were most likely due to shrinkage of hydrophilic shells upon drying samples.

CMC is one of the most physicochemical parameter of the micellization behavior of amphiphilic copolymers in dilute aqueous solution. The CMC of mPEG-b-(PCL-*g*-P(DA-*co*-DMAEMA)) in water was determined by fluorescence technique with pyrene as a probe summarized in Table 2. The CMC values of mPEG-b-(PCL-*g*-P(DA_{30}-*co*-$DMAEMA_{10}$)), mPEG-b-(PCL-*g*-P(DA_{30}-*co*-$DMAEMA_{15}$)) and mPEG-b-(PCL-*g*-P(DA_{30}-*co*-$DMAEMA_{20}$)) were determined to be 3.4 μg/mL, 3.6 μg/mL and 3.2 μg/mL, respectively. The results show that different structure of mPEG-b-(PCL-*g*-P(DA-*co*-DMAEMA)) micelles containing the same stability of self-assembly. It was worth pointing out that the content of the hydrophilic

DMAEMA moieties only slightly affected the CMC, which may be because the DMAEMA moieties was in the core of micelles and the main driving force behind the formation of micelles in water is the hydrophobic interactions of hydrophobic moieties[36]. Therefore, the DMAEMA in the core was weak protonation at pH 7.4. Furthermore, the zeta potential of mPEG-b-(PCL-*g*-P(DA-*co*-DMAEMA)) micelles was no different at pH 7.4, indicating that the moieties of DMAEMA of micelles was in the core and little protonation.

3.3. Dual-pH dependent hydrolysis monitored by ^{1}H-NMR, laser particle size analyzer and an optical analyzer Turbiscan.

The pH-dependent hydrolysis behaviors of the freeze-dried micelles dispersed in D_2O were studied by ^{1}H-NMR at pH 5.0 as shown in Fig. 3. At the first 4 h of hydrolysis, proton signals of the hydrophobic block of all the copolymers were weak (Fig. 3A). This was because the typical micelles structure made the proton of hydrophobic block trapped in the core and shielded by the mPEG shell. During the incubation period, the proton signals of the hydrophobic moieties in PCL-*g*-P(DA-*co*-DMAEMA) were gradually observed because the micelles were partly dissociated into unimers. Thus the intensity increase of the peak of moieties PCL-*g*-P(DA-*co*-DMAEMA) (at 1.4 ppm) could be used to monitor hydrolysis degree. Compared to mPEG-b-(PCL-*g*-P(DA_{30}-*co*-$DMAEMA_{10}$)), hydrolysis of the mPEG-b-(PCL-*g*-P(DA_{30}-*co*-$DMAEMA_{20}$)) with more DMAEMA moieties was faster (Fig. 3C and D). These results showed the hydrolysis of the pendent ketal could be accelerated by the effect of DMAEMA. We speculated that protonation of DMAEMA moieties in acidic medium leaded to an increase in hydrophilicity. Thus, more water molecules and hydronium ions could be absorbed into the core of micelles. Hydrolysis of the ketal moieties was enhanced. To verify this, we studied the zeta potential of the freeze-dried micelles dispersed in H_2O at pH 5.0 as shown in Fig. S2. At the same time point (2 h, 4 h or 24 h), the zeta potential was increased with the amount of DMAEMA in the mPEG-b-(PCL-*g*-P(DA-*co*-DMAEMA)) micelles. Furthermore, the polymer chains of P(DA-*co*-DMAEMA) collapse into compact “globules”

conformation at pH 7.4 , while expanded stretched conformation occurs by protonation of DMAEMA moieties at pH 5.0, which leaded to the repulsive interaction among the polymer chains. Therefore, the expanded core of the mPEG-b-(PCL-*g*-P(DA-*co*-DMAEMA)) micelles by the protonation DMAEMA moieties resulted more water into the core of the micelles, as a result the hydrolysis of the ketal moieties is enhanced[37].

The dual-pH dependent hydrolysis of mPEG-b-(PCL-*g*-PDA) and mPEG-b-(PCL-*g*-P(DA-*co*-DMAEMA)) micelles at pH 7.4 and 5.0 was monitored by an optical analyzer Turbiscan. The variation of backscattering data (ΔBS), depended on the mean particle size and their volume fraction, can be used to reflect the dual-pH dependent hydrolysis rate of micelles. Firstly, the stability of mPEG-b-(PCL-*g*-P(DA_{30}-*co*-$DMAEMA_{20}$)) micelles was measured because the physiological and biological stability of polymeric micelles is of particular importance for their pharmaceutical applications. As shown in Fig. 3E, the ΔBS profiles remained close to the base line value were observed for mPEG-b-(PCL-*g*-P(DA_{30}-*co*-$DMAEMA_{20}$)) micelles at pH 7.4 during the entire time of analysis. This finding showed that no creaming or sedimentation occurred during the entire time indicating the high stability of mPEG-b-(PCL-*g*-P(DA_{30}-*co*-$DMAEMA_{20}$)) micelles at pH 7.4. Furthermore, In view of the potential utility of micelles formulation for pharmaceutical applications, stability is significant for long-term storage, transportation, and scalable processing. As shown in Table S1, stability study was carried out by re-dissolving micelles in PBS at 37 ^{o}C for 3 days to assess the size change. The stability of the nanoparticles as drug carriers in PBS containing serum or proteins is also important. As shown in Table S1, the particle size of micelles did not change distinctly in 3 day in PBS containing 10% (v/v) FBS. Different dual-pH dependent hydrolysis behavious of mPEG-b-(PCL-*g*-P(DA-*co*-DMAEMA)) micelles at pH 5.0 were observed as shown in Fig. 3F, 4G and 4H. As shown in Fig. 3F, the ΔBS profiles of mPEG-b-(PCL-g-P(DA_{30}-*co*-$DMAEMA_{10}$)) were slightly increased, indicating a decrease in micelles stability. Especially, the ΔBS profiles of mPEG-b-(PCL-g-P(DA_{30}-*co*-$DMAEMA_{20}$)) increased gradually to 6 %

indicating the appearance of more abundant aggregation as shown in Fig. 3H compared with the the ΔBS profiles of mPEG-b-(PCL-g-P(DA_{30}-*co*-$DMAEMA_{15}$)) as shown in Fig. 3G. In particular, mPEG-b-(PCL-*g*-P(DA_{30}-$DMAEMA_{20}$)) micelles showed a high instability due to a fast hydrolysis rate of micelle.

The effect of ketal hydrolysis in the side-chain on the average size of the mPEG-b-(PCL-*g*-P(DA-*co*-DMAEMA)) micelles was probed as shown in Fig. 4. As expected, the average sizes of all four copolymers micelles remained almost unchanged throughout 12 h at pH 7.4 (Fig. 4A). Under the conditions of pH 6.5, mPEG-b-(PCL-*g*-PDA) and mPEG-b-(PCL-*g*-P(DA_{30}-*co*-$DMAEMA_{10}$)) micelles showed slightly increase in micelle sizes and maintained a low PDI as shown in Fig. 4B. In contrast, the remarkable sizes change of mPEG-b-(PCL-*g*-P(DA_{30}-*co*-$DMAEMA_{15}$)) and mPEG-b-(PCL-*g*-P(DA_{30}-*co*-$DMAEMA_{20}$)) micelles were observed with the PDI 0.41 and 0.55, respectively. Hydrophobic DA side chains of mPEG-b-(PCL-*g*-P(DA-*co*-DMAEMA)) bearing acetal groups can be selectively hydrolyzed into a hydrophilic side chains with hydroxyl groups in the acidic environment [38]. This process can be enhanced by the DMAEMA moieties in copolymers due to the protonation of DMAEMA moieties in acidic medium leaded to an increase in hydrophilicity. Furthermore, at pH 5.0, a large number of 20 nm particles of mPEG-b-(PCL-*g*-P(DA_{30}-*co*-$DMAEMA_{20}$)) copolymer were detected as a result of dissociation, which was agree with the result of the pH-dependent hydrolysis studies in Fig. 3. Zhong had reported that the acetal groups can be hydrolyzed into a hydrophilic side chains with hydroxyl groups in the acidic environment which may lead to the swell of micelles. Furthermore, with the time increasing, the swell micelles disassembled [39, 40]. In summary, it was clearly shown that acid-triggered ketal side-chain hydrolysis was directly impacted by the length of the DMAEMA moieties.

3.4. Loading and *in vitro* release of DOX.

DOX-loaded micelles were prepared at a polymer concentration of 1 mg/mL and DOX was loaded into mPEG-b-(PCL-*g*-PDA) and mPEG-b-(PCL-*g*-P(DA-*co*-DMAEMA)) micelles.

The characteristic of the DOX-loaded micelles, including size, size distribution, loading content and encapsulation efficiency were summarized in Table 2. All the PDI remained in a narrow range of 0.12-0.13. Compared with mPEG-b-(PCL-*g*-PDA), mPEG-b-(PCL-*g*-P(DA-*co*-DMAEMA)) micelles showed a much higher drug loading capacity. The drug loading content and encapsulation efficiency of mPEG-b-(PCL-*g*-P(DA-*co*-DMAEMA)) micelles were nearly 2 times higher than that of mPEG-b-(PCL-*g*-PDA) micelles. Moreover, the drug loading content and encapsulation efficiency of mPEG-b-(PCL-*g*-P(DA-*co*-DMAEMA)) micelles increased with increasing the content of DMAEMA units. These phenomena can be due to the intramolecular aggregation mechanism, the introduction of DMAEMA groups decreased the crystyalization of PCL segments and created a steric barrier around PCL core, thus leading to forming looser and larger aggregates, perhaps giving rise to greater drug encapsulation abilities[41]. This result agreed with the size distrubution of mPEG-b-(PCL-*g*-P(DA-*co*-DMAEMA)) micelles as shown in Fig. 2.

The *in vitro* release of DOX from mPEG-b-(PCL-*g*-P(DA-*co*-DMAEMA)) micelles was investigated at 37 ^{o}C under the condition of pH 7.4, 6.5 and 5.0, respectively. As shown in Fig. 4D, the release of DOX form mPEG-b-(PCL-*g*-P(DA-*co*-DMAEMA)) micelles was largely inhibited, in which only about 6 % was released in 12 h at pH 7.4. These results indicated that the structure of mPEG-b-(PCL-*g*-P(DA-*co*-DMAEMA)) containing DMAEMA moieties had high stability at physiological condition. However, as shown in Fig. 4E, the release of DOX from mPEG-b-(PCL-*g*-P(DA_{30}-*co*-$DMAEMA_{20}$)) micelles was significantly accelerated at pH 6.5 with 59 % compared with the release from mPEG-b-(PCL-*g*-PDA) with 19 % in 12 h. It was interesting to note that the moieties of DMAEMA of mPEG-b-(PCL-*g*-P(DA_{30}-*co*-$DMAEMA_{20}$)) copolymer significantly enhanced the acid-triggered ketal side-chain hydrolysis resulting in the swelling and disassembly of mPEG-b-(PCL-*g*-P(DA_{30}-*co*-$DMAEMA_{20}$)) micelles. This was consistent with the observation that mPEG-b-(PCL-*g*-P(DA_{30}-*co*-$DMAEMA_{20}$)) micelles were rapidly destabilized under pH 6.5 as shown in Fig. 3.

These results clearly indicated that protonation of the DMAEMA moieties in acidic medium resulted in an increase in their hydrophilicity, enhancing the uptake of water molecules and hydronium ions into the nanoparticles to speed up hydrolysis of the ketal moieties [42]. Especially, it can be observed that the DOX release rate at pH 5.0 from mPEG-b-(PCL-*g*-P(DA_{30}-*co*-$DMAEMA_{20}$)) micelles was extremely high. The cumulative release of DOX was approximately 88% in 12 h. The drug release behavior from polymeric micelles depended on drug diffusion rate from the micelles, micelles stability and the interaction between the drug and the core-forming block. The significant increase in DOX release from mPEG-b-(PCL-*g*-P(DA_{30}-*co*-$DMAEMA_{20}$)) micelles in the acidic medium can be ascribed to that the dual pH-induced hydrolysis of the DA as demonstrated above. Owing to the protonation DMAEMA moieties, a repulsive electrostatic force will generate in the DOX-loaded mPEG-b-(PCL-*g*-P(DA_{30}-*co*-$DMAEMA_{20}$)) micelles, which can greatly accelerate the release rate of drug. It should further be pointed out that drug release rate slightly decreased with increasing DMAEMA content in mPEG-b-(PCL-*g*-P(DA_{30}-*co*-$DMAEMA_{20}$)) copolymers.

3.5. Cellular internalization of mPEG-b-(PCL-*g*-P(DA-*co*-DMAEMA)) micelles dual-loaded with DiO and DiI.

A fluorescence resonance energy transfer (FRET) pair, DiO and DiI, was physically loaded into the inner core of mPEG-b-(PCL-*g*-P(DA-*co*-DMAEMA)) micelles to study the physiological and biological stability of polymeric micelles *in vitro*. For micelles with both DiO (donor, Ex/Em 488/501 nm) and DiI (acceptor, Ex/Em 501/565 nm) inside, when they are excited at wavelength of 488 nm, the energy generated from DiO can be transferred to DiI. Upon release of the FRET pair from micelles, the distance between the FRET pair increased (>10 nm), resulting in decreased emission at 565 nm of DiI[43, 44].Therefore, the stress of emission at 565 nm could be used to evaluate the integrity of micelles. The characteristics of the FRET micelles were analyzed as shown in Table S1. Furthermore, the difference in the mPEG-b-(PCL-*g*-P(DA-*co*-DMAEMA)) micelles with a series of DMAEMA moieties could

be revealed. As shown in Fig. 5A, after MCF-7s cells were incubated with mPEG-b-(PCL-*g*-P(DA-*co*-DMAEMA)) micelles for 4 h, FRET from DiO to DiI occurred at the lysosome The FRET efficiency at the lysosome was gradually decreased with the increasing the length of DMAEMA moieties in the micelles from mPEG-b-(PCL-*g*-PDA) to mPEG-b-(PCL-*g*-P(DA_{30}-*co*-$DMAEMA_{20}$)). This decreased in the intensity was due to the release of the probes from the micelles in acid lysosome environment. These results showed the hydrolysis of the pendent ketal could be accelerated by the effect of DMAEMA. A statistic of co-location ratio of DiI with lysosome was carried out by counting pixels of yellow (signals of DiI) and yellow and green (signals presented lysotracker green) in each picture and was calculated as:

$$\text{Co} - \text{location ration } (\%) = \left(\frac{\text{Counts yellow}}{\text{Counts yellow} + \text{Counts green}}\right) \times 100$$

As shown in Fig. 5C, the co-location ratio of yellow signals in the cell incubated different mPEG-b-(PCL-*g*-P(DA-*co*-DMAEMA)) micelles gradually decreased from mPEG-b-(PCL-*g*-PDA_{30}) to mPEG-b-(PCL-*g*-P(DA_{30}-*co*-$DMAEMA_{20}$)) indicating that the hydrolysis of micellles can be enhanced by the DMAEMA moieties in copolymers due to the protonation of DMAEMA moieties in acidic medium leaded to an increase in hydrophilicity. Then the rate of DA was enhanced in the acid environment. The time resolved spectra were re-organized to show the FRET ratio as a function of incubation time (Fig. 5D). During the incubation period, the FRET ratio $I_{DiI}/(I_{DiI}/I_{DiO})$ of the mPEG-b-(PCL-*g*-P(DA_{30}-*co*-$DMAEMA_{20}$)) micelles rapidly decreased from 0.95 to 0.33 due to structural dissociation whereas the FRET ratio of the mPEG-b-(PCL-*g*-PDA) micelles gradually reduced from 0.91 to 0.81, reflecting the release of hydrophobic probes from micelles mediated by the moieties of DMAEMA. These results collectively show that the hydrolysis of the pendent ketal could be accelerated by DMAEMA.

3.6. Intracellular DOX release and antitumor activity.

The cellular uptake and intracellular drug release profiles of DOX-loaded mPEG-b-(PCL-*g*-P(DA-*co*-DMAEMA)) micelles were investigated in MCF-7 cells using CLSM. Here, the red

fluorescence signal from the DOX was used for the fluorescence imaging of cells. As shown in Fig. 6A, after 4 h incubation, stronger DOX fluorescence appeared both in the cytoplasm and in the nucleus of MCF-7 cells for free DOX than the DOX-loaded micelles. It had been known DOX molecule is membrane permeable and can be internalized into tumor cells through a passive diffusion mechanism while the DOX-loaded micelles need to be endocytosed [45-47]. After incubation time of 4 h with DOX-loaded mPEG-b-(PCL-*g*-P(DA_{30}-*co*-$DMAEMA_{20}$)) micelles, DOX had mostly released into the nuclei region of cells, which was notably higher than that incubated with DOX-loaded mPEG-b-(PCL-*g*-PDA) micelles. This different intracellular drug release behaviors between DOX-loaded mPEG-b-(PCL-*g*-P(DA_{30}-*co*-$DMAEMA_{20}$)) and mPEG-b-(PCL-*g*-PDA) micelles were mostly due to fast DOX release from mPEG-b-(PCL-*g*-P(DA_{30}-*co*-$DMAEMA_{20}$)) micelles following escaping from endosomes as a result of rapidly hydrolysis of the ketal moieties within the moieties of DMAEMA. Moreover, after incubation of 12 h, Fig. S3 shows that stronger DOX fluorescence appeared in the nuclei of MCF 7 cells for mPEG-b-(PCL-*g*-P(DA_{30}-*co*-$DMAEMA_{20}$)) micelles than mPEG-b-(PCL-*g*-PDA). Interestingly, as shown in Fig. 6A (b, c, and d), the location of DOX red fluorescence with the nucleus blue fluorescence was increased with increased DMAEMA moieties in mPEG-b-(PCL-*g*-P(DA-*co*-DMAEMA)) micelles from mPEG-b-(PCL-*g*-P(DA_{30}-*co*-$DMAEMA_{10}$)) micelles to mPEG-b-(PCL-*g*-P(DA_{30}-*co*-$DMAEMA_{20}$)) micelles. These results were also agreed with the result in Fig. 4 that the *in vitro* release of DOX from mPEG-b-(PCL-*g*-P(DA_{30}-*co*-$DMAEMA_{20}$)) was faster than mPEG-b-(PCL-*g*-PDA) micelles. Thus the DMAEMA moieties in the mPEG-b-(PCL-*g*-P(DA_{30}-*co*-$DMAEMA_{20}$)) micelles could enhance the speed of hydrolysis of the ketal moieties due to the the protonation of DMAEMA moieties in acidic medium leaded to an increase in hydrophilicity. Therefore, the speed of hydrolysis of mPEG-b-(PCL-*g*-P(DA_{30}-*co*-$DMAEMA_{20}$)) could be well controlled through adjusting the length of DMAEMA moieties in the copolymers. An Flow Cytometry (FCM) assay was performed to evaluate and compare

the cellular uptake of DOX loaded mPEG-b-(PCL-*g*-P(DA-*co*-DMAEMA)) and mPEG-b-(PCL-*g*-PDA)micelles. As shown in Fig. 6B, the fluorescence intensity of DOX were about the same height for all four polymer micelles at the same time point, indicating that there is no difference in cell uptake for mPEG-b-(PCL-*g*-P(DA_{30}-*co*-$DMAEMA_{10}$)), mPEG-b-(PCL-*g*-P(DA_{30}-*co*-$DMAEMA_{15}$)), mPEG-b-(PCL-*g*-P(DA_{30}-*co*-$DMAEMA_{20}$)), and mPEG-b-(PCL-*g*-PDA) micellles. However, as shown in Fig. 6A, the results clearly indicated that the red fluorescence signal from the DOX in cell nucleus incubated in mPEG-b-(PCL-*g*-P(DA_{30}-*co*-$DMAEMA_{20}$)) micelles was stronger than the mPEG-b-(PCL-*g*-PDA). This result shown that the ability of cell uptake of mPEG-b-(PCL-*g*-P(DA_{30}-*co*-$DMAEMA_{20}$)) and mPEG-b-(PCL-*g*-PDA) micelles was equal, but the drug release from micelles after uptake into cell was different. Thus, after uptake into cell, the fast DOX relase from mPEG-b-(PCL-*g*-P(DA_{30}-*co*-$DMAEMA_{20}$)) micelles than mPEG-b-(PCL-*g*-PDA) occured due to the enhanced hydrolysis of the ketal moieties by protonaitno of DMAEMA. Notice of the discrepancy between cellular uptake and drug delivery intracellar efficiency of these micelles, uptake mechanism of these micelles was investigated. As shown in Fig. S4, cellular uptake of mPEG-b-(PCL-*g*-PDA), mPEG-b-(PCL-*g*-P(DA_{30}-$DMAEMA_{10}$)), mPEG-b-(PCL-*g*-P(DA_{30}-$DMAEMA_{15}$)) and mPEG-b-(PCL-*g*-P(DA_{30}-$DMAEMA_{20}$)), decreased after treated with different endocytosis inhibitors, indicating that micelles entered cells by endocytosis. However, the cellular uptake inhibition to these micelles was no different, indicating that these micelles entered into cells by the same diffusion mechanism.

Furthermore, in order to precisely affirm the DOX content in cells and nucleus after incubated DOX loaded mPEG-b-(PCL-*g*-P(DA_{30}-$DMAEMA_{20}$)) and mPEG-b-(PCL-*g*-PDA) micelles, the DOX was extracted from the MCF-7 cells which was tested by high performance liquid chromatography (HPLC) as shown in Fig. 6C. As shown in Fig. 6D, the DOX concentration in nuclear of MCF-7 cells was also test by HPLC. The DOX concentration in nuclear increased from mPEG-b-(PCL-*g*-PDA) to mPEG-b-(PCL-*g*-P(DA_{30}-*co*-$DMAEMA_{20}$))

indicating that more DOX release from the mPEG-b-(PCL-*g*-P(DA_{30}-*co*-$DMAEMA_{20}$)) micelles than others which was correspondence with the result of CLSM in Fig. 6A and FCM in Fig. 6B. In a sum, these results demonstrated that dual-pH triggered micelles for intracellular drug delivery could significantly facilitate endo-lysosomal escape due to the enhanced hydrolysis of the ketal moieties, leading to a high therapeutic efficacy.

3.7. *In vitro* and *In vivo* anticancer efficacy.

The cytotoxicity of mPEG-b-(PCL-*g*-PDA) and mPEG-b-(PCL-*g*-P(DA_{30}-*co*-$DMAEMA_{20}$)) micelles was investigate in MCF-7 and 4T1 cells by MTT assays. The result revealed that mPEG-b-(PCL-*g*-PDA) and mPEG-b-(PCL-*g*-P(DA_{30}-*co*-$DMAEMA_{20}$)) micelles were practically non-toxic (cell viabilities > 85 %) up to a test concentration of 1.0 mg/mL (Fig. 7A), confirming that these degradable micelles had good biocompatibility [48, 49].

The antitumor activity of DOX-loaded mPEG-b-(PCL-*g*-PDA) and mPEG-b-(PCL-*g*-P(DA_{30}-*co*-$DMAEMA_{20}$)) micelles were studied in MCF-7 and 4T1 cells. It could be noted that DOX-loaded mPEG-b-(PCL-*g*-P(DA_{30}-*co*-$DMAEMA_{20}$)) micelles had lower IC50 (half inhibitory concentration) values than DOX-loaded mPEG-b-(PCL-*g*-PDA) micelles (MCF-7: 2.5 μg/mL for DOX-loaded mPEG-b-(PCL-*g*-P(DA-*co*-DMAEMA)) micelles and 6.5 μg/mL for DOX-loaded mPEG-b-(PCL-*g*-PDA) micelles; 4T1: 2.1μg/mL for DOX-loaded mPEG-b-(PCL-*g*-P(DA_{30}-*co*-$DMAEMA_{20}$)) and 7.5μg/mL for mPEG-b-(PCL-*g*-PDA). The higher anti-tumor activity of DOX-loaded mPEG-b-(PCL-*g*-P(DA_{30}-*co*-$DMAEMA_{20}$)) micelles was attributed to the rapid release of DOX from micelles which accelerated the diffusion and aggregation of DOX from the cytoplasm to the nuclei which was accordance with the results of Fig. 6. This result demonstrates the DOX release from mPEG-b-(PCL-*g*-P(DA_{30}-*co*-$DMAEMA_{20}$)) micelles was enhanced due to the endo-/lysosomal pH-responsibility of PDA with DMAEMA. Thus it could be summarized that synergistic dual-pH response mPEG-b-(PCL-*g*-P(DA_{30}-*co*-$DMAEMA_{20}$)) micelles possessed the rapid acid catalyzed hydrolysis feature. This result was in accordance with the CLSM observations that mPEG-b-(PCL-*g*-P(DA_{30}-*co*-$DMAEMA_{20}$))

micelles mediate fast intracellular drug release as compared to corresponding mPEG-b-(PCL-*g*-PDA) micelles.

To evaluate the *in vivo* antitumor efficacy of synergistic pH response micelles, saline, DOX, DOX-loaded mPEG-b-(PCL-*g*-PDA) and mPEG-b-(PCL-*g*-P(DA_{30}-*co*-$DMAEMA_{20}$)) micelles were injected, every two days, into 4T1 tumor-bearing Balb-c mice via the lateral tail vein. As shown in Fig. 7E, saline treatments did not have any substantial effect on the tumor growth, and the tumor volumes increased rapidly. As compared with saline treatments, the tumor growth was effectively inhibited in all the groups treated with free DOX, DOX-loaded mPEG-b-(PCL-*g*-PDA) micelles and DOX-loaded mPEG-b-(PCL-*g*-P(DA_{30}-*co*-$DMAEMA_{20}$)) micelles until 12 days after injection. Notably, the tumor volume treated with DOX-loaded mPEG-b-(PCL-*g*-P(DA_{30}-*co*-$DMAEMA_{20}$)) micelles was remarkably more decreased. This result suggested that the synergistic dual-pH response mPEG-b-(PCL-*g*-P(DA_{30}-*co*-$DMAEMA_{20}$)) micelles maintained high drug potency against the cancer cells. At 20 days after injection, the DOX-loaded mPEG-b-(PCL-*g*-P(DA_{30}-*co*-$DMAEMA_{20}$)) micelles exhibited enhanced anti-cancer activity over the DOX-loaded mPEG-b-(PCL-*g*-PDA) micelles.

To evaluate the cytotoxicity of micelles, the body weight of mice was measured. As shown in Fig. 7F, the DOX-loaded mPEG-b-(PCL-*g*-PDA) and DOX-loaded mPEG-b-(PCL-*g*-P(DA_{30}-*co*-$DMAEMA_{20}$)) micelles treatment resulted in almost no difference in the physiological activity level and body weight after 20 days.

3.8. *In vivo* Biodistribution and Tumor Accumulation

To evaluate tissue distributions, DOX loaded mPEG-b-(PCL-*g*-PDA) and mPEG-b-(PCL-*g*-P(DA_{30}-*co*-$DMAEMA_{20}$)) micelles at the same DOX dose (5 mg/kg) were intravenously injected into 4T1 tumor-bearing mice, the time dependent tumor accumulation and tissue distribution were observed via fluorescence imaging of DOX. After injection, the major organs (heart, liver, spleen, lungs, kidney, and tumor tissues) were isolated for observation of

ex vivo images and the fluorescence intensity was quantitatively analyzed. As shown in Fig. 7G, it is interesting to note that the fluorescence signal of DOX loaded mPEG-b-(PCL-*g*-P(DA_{30}-*co*-$DMAEMA_{20}$)) micelles in tumors was equal to DOX loaded mPEG-b-(PCL-*g*-PDA) micelles, which was attributed to the same tumor accumulation of DOX loaded micelles. It had been known that the nanocarriers accumulated in tumor tissue by the EPR effect. The stability of the polymer micelles in blood circulation is an important issue to affect their accumulation. Therefore, c mPEG-b-(PCL-*g*-P(DA_{30}-*co*-$DMAEMA_{20}$)) micelles with excellent stability and inhibition in DOX wastage as well as mPEG-b-(PCL-*g*-PDA) micelles in blood circulation could definitely deliver payload in tumor tissue.

3.9. Histomorphological analysis.

H&E assays were executed to study the toxicology and the antitumor efficacy of the DOX-loaded mPEG-b-(PCL-*g*-PDA) and mPEG-b-(PCL-*g*-P(DA_{30}-*co*-$DMAEMA_{20}$)) micelles. Liver and spleen are the reticuloendothelial system (RES) organs and the nanosized materials preferentially distribute in these organs after intravenous injection. Kidney is the elimination organ of most micelles. Hence, liver, spleen and kidney were collected for the *in vivo* toxicity studies. H&E results showed in Fig. 7H suggested that there were no pathological changes in liver, spleen and kidney in both mPEG-b-(PCL-*g*-PDA) and mPEG-b-(PCL-*g*-P(DA_{30}-*co*-$DMAEMA_{20}$)) micelles groups, indicating the safety of our DOX loaded micelles *in vivo*. The breast cancer xenograft images in Fig. 7H revealed that the largest area of apoptotic or necrosis cells (with broken nucleis) was found in mPEG-b-(PCL-*g*-P(DA_{30}-*co*-$DMAEMA_{20}$)) micelles groups, which was in accordance with the best *in vivo* antitumor effect of mPEG-b-(PCL-*g*-P(DA_{30}-*co*-$DMAEMA_{20}$)) micelles micelles groups in Fig. 7A. These results indicated clearly that the tumor inhibition ability of DOX was significantly enhanced by dual-pH responsive mPEG-b-(PCL-*g*-P(DA_{30}-*co*-$DMAEMA_{20}$)) micelles groups encapsulation.

4. Conclusion

Synergistic dual-pH response moieties, a pH solubility switch moietie (DMAEMA) and a pH labile ketal group were incorporated into the amphiphilic copolymer which can be formulated into micelles with tunable fast degradation in acid environment and high stability in physiological condition. The improved protonation of DMAEMA moieties at acidic condition could switch the polymeric micelles cores from hydrophobic to hydrophilic then increase the uptake of water into the core of the micelles. Furthermore, the polymer chains of P(DA-*co*-DMAEMA) collapse into compact "globules" conformation at pH 7.4, while the polymer chains of P(DA-*co*-DMAEMA) by protonation are in the expanded stretched conformation at pH 6.8, which also leading to the repulsive interaction among the polymer chains. Therefore, the core of the mPEG-b-(PCL-*g*-P(DA-*co*-DMAEMA)) micelles was expand by the protonation DMAEMA moieties resulting more water into the core of the micelles. Thus the hydrolysis of ketal groups could be accelerated, which was demonstrated by monitoring the stability of mPEG-b-(PCL-*g*-P(DA-*co*-DMAEMA)) micelles under acid condition using ^{1}H-NMR and an optical analyzer Turbiscan. The drug release profile of DOX also shown that the hydrolysis speed of mPEG-b-(PCL-*g*-P(DA-*co*-DMAEMA)) micelles accelerated by adding the DMAEMA moieties into the copolymer. Furthermore, *in vivo* anti-tumor efficacy experiment confirmed that the mPEG-b-(PCL-*g*-P(DA_{30}-$DMAEMA_{20}$)) micelles with more DMAEMA moieties than mPEG-b-(PCL-*g*-PDA) micelles had a high anti-tumor efficiency.

Acknowledgements

This research was financially supported by National Natural Science Foundation of China (31470963, 81371667, 81471727).

References

1. Z. Zhou, L. Li, Y. Yang, X. Xu and Y. Huang, *Biomaterials*, 2014, **35**, 6622-6635.
2. H. Wei, R.-X. Zhuo and X.-Z. Zhang, *Progress in Polymer Science*, 2013, **38**, 503-535.
3. Y. Shen, E. Jin, B. Zhang, C. J. Murphy, M. Sui, J. Zhao, J. Wang, J. Tang, M. Fan and E. Van Kirk, *Journal of the American Chemical Society*, 2010, **132**, 4259-4265.
4. H. Deng, Y. Zhang, X. Wang, Y. Cao, J. Liu, J. Liu, L. Deng and A. Dong, *Acta biomaterialia*, 2015, **11**, 126-136.
5. X. Gao, S. Wang, B. Wang, S. Deng, X. Liu, X. Zhang, L. Luo, R. Fan, M. Xiang and C. You, *Biomaterials*, 2015, **53**, 646-658.
6. J.-Z. Du, X.-J. Du, C.-Q. Mao and J. Wang, *Journal of the American Chemical Society*, 2011, **133**, 17560-17563.
7. E. A. Mahmoud, J. Sankaranarayanan, J. M. Morachis, G. Kim and A. Almutairi, *Bioconjugate Chemistry*, 2011, **22**, 1416-1421.
8. S. E. Paramonov, E. M. Bachelder, T. T. Beaudette, S. M. Standley, C. C. Lee, J. Dashe and J. M. J. Fréchet, *Bioconjugate Chemistry*, 2008, **19**, 911-919.
9. K. Schwach-Abdellaoui, A. Monti, J. Barr, J. Heller and R. Gurny, *Biomaterials*, 2001, **22**, 1659-1666.
10. Z. Chen, L. Zhang, Y. Song, J. He, L. Wu, C. Zhao, Y. Xiao, W. Li, B. Cai and H. Cheng, *Biomaterials*, 2015, **52**, 240-250.
11. T. D. Knab, S. R. Little and R. S. Parker, *Journal of Controlled Release*, 2015.
12. X. Huang, F. Du, J. Cheng, Y. Dong, D. Liang, S. Ji, S.-S. Lin and Z. Li, *Macromolecules*, 2009, **42**, 783-790.
13. C. Oerlemans, W. Bult, M. Bos, G. Storm, J. F. W. Nijsen and W. E. Hennink, *Pharmaceutical Research*, 2010, **27**, 2569-2589.
14. R. Tang, W. Ji, D. Panus, R. N. Palumbo and C. Wang, *Journal of Controlled Release*, 2011, **151**, 18-27.
15. Z.-Y. Qiao, F.-S. Du, R. Zhang, D.-H. Liang and Z.-C. Li, *Macromolecules*, 2010, **43**, 6485-6494.
16. W. Chen, F. Meng, F. Li, S.-J. Ji and Z. Zhong, *Biomacromolecules*, 2009, **10**, 1727-1735.
17. Q. Zhang, Z. Hou, B. Louage, D. Zhou, N. Vanparijs, B. G. De Geest and R. Hoogenboom, *Angewandte Chemie*, 2015, **127**, 11029-11033.
18. R. A. Shenoi, J. K. Narayanannair, J. L. Hamilton, B. F. L. Lai, S. Horte, R. K. Kainthan, J. P. Varghese, K. G. Rajeev, M. Manoharan and J. N. Kizhakkedathu, Journal of the American Chemical Society, 2012, **134**, 14945-14957.
19. W. Chen, M. Zheng, F. Meng, R. Cheng, C. Deng, J. Feijen and Z. Zhong, *Biomacromolecules*, 2013, **14**, 1214-1222.
20. Z.-Y. Qiao, R. Ji, X.-N. Huang, F.-S. Du, R. Zhang, D.-H. Liang and Z.-C. Li, *Biomacromolecules*, 2013, **14**, 1555-1563.
21. M. D. Pluth, R. G. Bergman and K. N. Raymond, The Journal of Organic Chemistry, 2009, **74**, 58-63.
22. M. Tang, Z. Yang, Z. Feng, J. Zhou, J. Liu, J. Liu, W. Wang, J. Zhao, A. Dong and L. Deng, Polymer Chemistry, 2015, **6**, 6671-6679.
23. E. M. Bachelder, T. T. Beaudette, K. E. Broaders, J. Dashe and J. M. Fréchet, Journal of the American Chemical Society, 2008, **130**, 10494-10495.
24. Q. Zhang, Z. Hou, B. Louage, D. Zhou, N. Vanparijs, B. G. De Geest and R. Hoogenboom, *Angewandte Chemie*, 2015, DOI: 10.1002/ange.201505145, n/a-n/a.
25. S. Brahim, D. Narinesingh and A. Guiseppi-Elie, *Biomacromolecules*, 2003, **4**, 1224-1231.
26. A. S. Lee, A. P. Gast, V. Bütün and S. P. Armes, *Macromolecules*, 1999, **32**, 4302-4310.
27. J.-F. Gohy, S. Antoun and R. Jérôme, *Macromolecules*, 2001, **34**, 7435-7440.
28. F. A. Plamper, A. Schmalz and A. H. E. Müller, *Journal of the American Chemical*

Society, 2007, **129**, 14538-14539.
29. F. A. Plamper, M. Ruppel, A. Schmalz, O. Borisov, M. Ballauff and A. H. Müller, *Macromolecules*, 2007, **40**, 8361-8366.
30. F. A. Plamper, J. R. McKee, A. Laukkanen, A. Nykanen, A. Walther, J. Ruokolainen, V. Aseyev and H. Tenhu, *Soft Matter*, 2009, **5**, 1812-1821.
31. D. Zhang, H. Zhang, J. Nie and J. Yang, *Polymer International*, 2010, **59**, 967-974.
32. G. Basu Ray, I. Chakraborty and S. P. Moulik, *Journal of Colloid and Interface Science*, 2006, **294**, 248-254.
33. C. Lemarchand, P. Couvreur, C. Vauthier, D. Costantini and R. Gref, *International Journal of Pharmaceutics*, 2003, **254**, 77-82.
34. Y. Sheng, C. Liu, Y. Yuan, X. Tao, F. Yang, X. Shan, H. Zhou and F. Xu, *Biomaterials*, 2009, **30**, 2340-2348.
35. T. Wei, C. Chen, J. Liu, C. Liu, P. Posocco, X. Liu, Q. Cheng, S. Huo, Z. Liang and M. Fermeglia, *Proceedings of the National Academy of Sciences*, 2015, **112**, 2978-2983.
36. J. Zhao, H. Wang, J. Liu, L. Deng, J. Liu, A. Dong and J. Zhang, *Biomacromolecules*, 2013.
37. F. Bossard, T. Aubry, G. Gotzamanis and C. Tsitsilianis, *Soft Matter*, 2006, **2**, 510-516.
38. J. Zhao, H. Wang, J. Liu, L. Deng, J. Liu, A. Dong and J. Zhang, *Biomacromolecules*, 2013, **14**, 3973-3984.
39. Y. Wu, W. Chen, F. Meng, Z. Wang, R. Cheng, C. Deng, H. Liu and Z. Zhong, *Journal of Controlled Release*, 2012, **164**, 338-345.
40. W. Chen, P. Zhong, F. Meng, R. Cheng, C. Deng, J. Feijen and Z. Zhong, *Journal of Controlled Release*, 2013, **169**, 171-179.
41. C. Hoskins, P. K. Thoo-Lin and W. P. Cheng, *Therapeutic Delivery*, 2011, **3**, 59-79.
42. K. Zhou, Y. Wang, X. Huang, K. Luby‐Phelps, B. D. Sumer and J. Gao, *Angewandte Chemie International Edition*, 2011, **50**, 6109-6114.
43. S. Jiwpanich, J.-H. Ryu, S. Bickerton and S. Thayumanavan, *Journal of the American Chemical Society*, 2010, **132**, 10683-10685.
44. H. Chen, S. Kim, L. Li, S. Wang, K. Park and J.-X. Cheng, *Proceedings of the National Academy of Sciences*, 2008, **105**, 6596-6601.
45. M. Li, Z. Tang, H. Sun, J. Ding, W. Song and X. Chen, *Polymer Chemistry*, 2013, **4**, 1199-1207.
46. Y. Pang, J. Liu, Y. Su, J. Wu, L. Zhu, X. Zhu, D. Yan and B. Zhu, *Polymer Chemistry*, 2011, **2**, 1661-1670.
47. J.-H. Ryu, S. Bickerton, J. Zhuang and S. Thayumanavan, *Biomacromolecules*, 2012, **13**, 1515-1522.
48. W. Song, Z. Tang, D. Zhang, Y. Zhang, H. Yu, M. Li, S. Lv, H. Sun, M. Deng and X. Chen, *Biomaterials*, 2014, **35**, 3005-3014.
49. S. Lv, Z. Tang, M. Li, J. Lin, W. Song, H. Liu, Y. Huang, Y. Zhang and X. Chen, *Biomaterials*, 2014, **35**, 6118-6129.

Fig. legends

Scheme 1. The illustration of the doxorubicin encapsulated into micelles and dual-pH responsive copolymer with fast acidic-degradation rate and high stability in physical condition.

Scheme 2. Synthesis of mPEG-b-(PCL-*g*-P(DA-*co*-DMAEMA))

Fig. 1 ^{1}H-NMR characterization of mPEG-b-(PCL-*g*-PDA) (A) and mPEG-b-(PCL-*g*-P(DA-*co*-DMAEMA)) (B)

Fig. 2 (A) Size distribution and TEM micrograph of mPEG-b-(PCL-*g*-PDA) (A), mPEG-b-(PCL-*g*-P(DA-*co*-DMAEMA$_{10}$)) (B) mPEG-b-(PCL-*g*-P(DA-*co*-DMAEMA$_{15}$)) (C) and mPEG-b-(PCL-*g*-P(DA-*co*-DMAEMA$_{20}$)) (D), scale bar 100 nm.

Fig. 3 Hydrolysis rate-DMAEMA content relationship cure measured by ^{1}H-NMR spectra of micelles in deuterated PB (pH 5.0) at different hydrolysis times. mPEG-b-(PCL-*g*-PDA) (A), mPEG-b-(PCL-*g*-P(DA$_{30}$-*co*-DMAEMA$_{10}$)) (B), and mPEG-b-(PCL-*g*-P(DA-*co*-DMAEMA$_{15}$)) (C) and mPEG-b-(PCL-*g*-P(DA$_{30}$-*co*-DMAEMA$_{20}$)) (D). Variation of backscattering data (ΔBS) of mPEG-b-(PCL-*g*-P(DA$_{30}$-*co*-DMAEMA$_{20}$)) at pH 7.4 measured for 12 h along the height axis of the sample tube (E) and mPEG-b-(PCL-*g*-P(DA$_{30}$-*co*-DMAEMA$_{10}$)) (F), mPEG-b-(PCL-*g*-P(DA$_{30}$-*co*-DMAEMA$_{15}$)) (G), and mPEG-b-(PCL-*g*-P(DA$_{30}$-*co*-DMAEMA$_{20}$)) (H) micelles at pH 5.0 measured for 12 h along the height axis of the sample tube.

Fig. 4 Time dependence of the size changes of mPEG-b-(PCL-*g*-PDA$_{30}$) (a), mPEG-b-(PCL-*g*-P(DA$_{30}$-*co*-DMAEMA$_{10}$)) (b), mPEG-b-(PCL-*g*-P(DA30-*co*-DMAEMA$_{15}$)) (c), and mPEG-b-(PCL-*g*-P(DA$_{30}$-*co*-DMAEMA$_{20}$)) (d) micelles at pH 7.4 (A), pH 6.5 (B) and pH 5.0 (C). pH triggered release of DOX from mPEG-b-(PCL-*g*-PDA$_{30}$), mPEG-b-(PCL-*g*-P(DA$_{30}$-*co*-DMAEMA$_{10}$)), mPEG-b-(PCL-*g*-P(DA$_{30}$-*co*-DMAEMA$_{15}$)), and mPEG-b-(PCL-*g*-P(DA$_{30}$-*co*-DMAEMA$_{20}$)) micelles during pH 7.4 (E), pH 6.5 (F) and pH 5.0 (G) at 37 ^{o}C.

Fig. 5 (A) Cellular internalization of mPEG-b-(PCL-*g*-PDA_{30}) (a), mPEG-b-(PCL-*g*-P(DA_{30}-*co*-$DMAEMA_{10}$)) (b), mPEG-b-(PCL-*g*-P(DA_{30}-*co*-$DMAEMA_{10}$)) (c), and mPEG-b-(PCL-*g*-P(DA_{30}-*co*-$DMAEMA_{20}$)) (d) micelles dual-loaded with DiO and DiI. MCF-7 cells were incubated with 100 μM micelles for 4 h (The scalbar 20 μm). (B) The enlarged view of 488 ex/DiI. (C) Statistics of co-located ratio of DiI with lysosome was carried out by counting pixels of yellow (signals of DiI) and yellow and green (signals presented by location of lysotracker green) in each picture. (D) Time-resolved spectra of MCF-7 cells incubated in micelles. FRET ratio, $I_{DiI}/(I_{DiI}/I_{DiO})$, as a function of incubation time. I_{DiI} and I_{DiO} represent the fluorescence intensities of DiI at 570 nm and DiO at 508 nm in the spectrum measurements. at 0 h, and I represent the ratio at 0.5, 1, 1.5 and 2 h.

Fig. 6 Intracellular uptake of DOX-loaded micelles. (A) Representative CLSM images of MCF-7 cells incubated with DOX-loaded mPEG-b-(PCL-*g*-PDA_{30}) micelles, DOX-loaded mPEG-b-(PCL-*g*-P(DA_{30}-*co*-$DMAEMA_{20}$)) micelles and free DOX (10 μg/mL) for 4 h (scale bars, 20 μm). (B) Intracellular fluorescence intensities of DOX-loaded mPEG-b-(PCL-*g*-PDA_{30}) (a), mPEG-b-(PCL-*g*-P(DA_{30}-*co*-$DMAEMA_{10}$)) (b), mPEG-b-(PCL-*g*-P(DA_{30}-*co*-$DMAEMA_{15}$)) (c), and mPEG-b-(PCL-*g*-P(DA_{30}-*co*-$DMAEMA_{20}$)) (d) micelles determined by flow cytometry. Statistical analysis of MFI and percentage of cell uptake were analyzed after gating, thus 10^5 viable cells were calculated, and all formulations were normalized to mock. Each bar represents the mean ± S.D. of three experiments. (C) HPLC results for cellular DOX concentration in MCF-7 cells incubated with DOX-loaded micelles and free DOX for 4 h. The results represent mean ± S.D. of three experiments. (D) HPLC results for cellular DOX concentration in nuclear of MCF-7 cells.

Fig. 7 Cytotoxicity of DOX-free mPEG-b-(PCL-*g*-PDA_{30}) (a) and mPEG-b-(PCL-*g*-P(DA_{30}-*co*-$DMAEMA_{20}$)) (d) micelles in MCF-7 cells (A) and in 4T1 cells (B). Anti-tumor activity of free DOX, DOX-loaded mPEG-b-(PCL-*g*-PDA_{30}) (a) and mPEG-b-(PCL-*g*-P(DA_{30}-*co*-$DMAEMA_{20}$)) (d) micelles in MCF-7 cells (C) and in 4T1 cells (D). The cells were incubated

with DOX-loaded micelles or free DOX for 24 h. Data are presented as the average ± standard deviation (n = 4)**.** *In vivo* anti-tumor efficacy of free DOX, DOX-loaded mPEG-b-(PCL-*g*-PDA_{30}) (a) and mPEG-b-(PCL-*g*-P(DA_{30}-*co*-$DMAEMA_{20}$)) (d) micelles in the 4T1 tumor bearing mice. (E) Tumor growth following treatment with DOX loaded micelles. (F) Mouse body weight during micelles treatment. * $p < 0.05$, ** $p < 0.01$. (G) Fluorescent image of tissue distribution of DOX loaded micelles micelles at 4 h-post injection. (H) Hematoxylin & eosin (H&E) assays of tumor and organs (liver, spleen and kidney) from mice that received different treatments. The scale bar was 50 μm

Table 1. Structure and composition of mPEG-b-(PCL-*g*-P(DA-*co*-DMAEMA))

Copolymers	DA : DMAEMA		M_n [a]	M_n [b]	PDI [b]
	Feed rate	Product[a]			
mPEG-b-(PCL_{65}-*co*-$BMPCL_{3.4}$)	-	-	12970	15200	1.24
mPEG-b-(PCL-*g*-PDA_{30})	30 :0	27:0	17470	18000	1.22
mPEG-b-(PCL-*g*-P(DA_{30}-*co*-$DMAEMA_{10}$))	30 :10	29:8	17100	18900	1.26
mPEG-b-(PCL-*g*-P(DA_{30}-*co*-$DMAEMA_{15}$))	30 :15	28: 12.8	17860	19100	1.30
mPEG-b-(PCL-*g*-P(DA_{30}-*co*-$DMAEMA_{20}$))	30 :20	28:19	18610	21600	1.28

65 and 3.4 is the theoretical number of monomers.
[a]Determined by ^{1}H-NMR.
[b]Determined by GPC.

Table 2. Characteristics of blank and DOX-loaded micelles mPEG-b-(PCL-*g*-P(DA-*co*-DMAEMA))

Copolymers	Blank micelles				DOX-loaded micelles[a]			
	Size (nm)[b]	CMC (mg/mL)[c]	PDI [b]	Zeta	Size (nm)	PDI	DLC (%)	DLE (%)
mPEG-b-(PCL-*g*-PDA_{30})	92 ± 3	0.9×10^{-3}	0.16	0	129 ± 8	0.13	3.7± 0.3	25± 0.1
mPEG-b-(PCL-*g*-P(DA_{30}-*co*-$DMAEMA_{10}$))	101 ± 5	3.4×10^{-3}	0.11	0.1	115 ± 5	0.12	4.5± 0.2	30± 0.1
mPEG-b-(PCL-*g*-P(DA_{30}-*co*-$DMAEMA_{15}$))	130 ± 3	3.6×10^{-3}	0.14	0.2	129 ± 2	0.13	5.6± 0.2	37± 0.2
mPEG-b-(PCL-*g*-P(DA_{30}-*co*-$DMAEMA_{20}$))	143 ± 4	3.2×10^{-3}	0.13	0.1	137 ± 3	0.12	6.6± 0.1	44± 0.1

[a]Free ratio of DOX to polymers was 15 mg/100 mg.
[b]Detetmined using laser particle size analyzer (zetasizer Nano ZS, Malvern Instruments) at 25 ^{o}C in PBS (10 mM, pH 7.4).
[c]Determined using pyrene as a fluorescence probe.

Scheme 1.

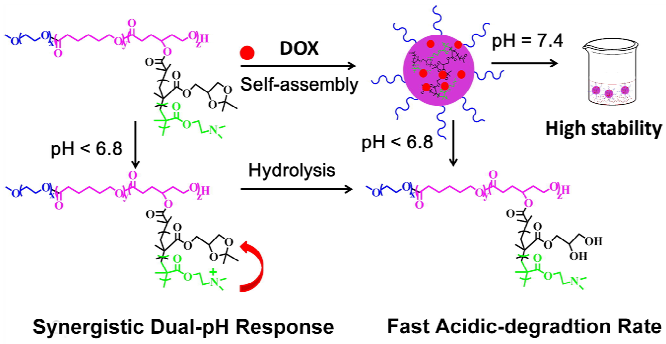

Scheme 2.

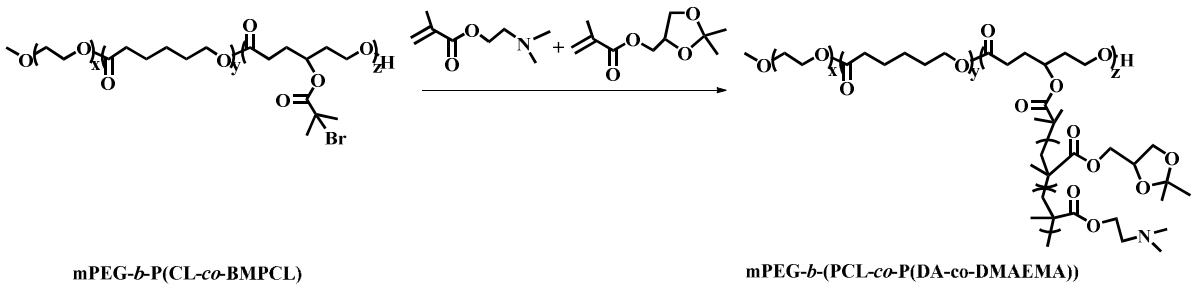

Fig. 1

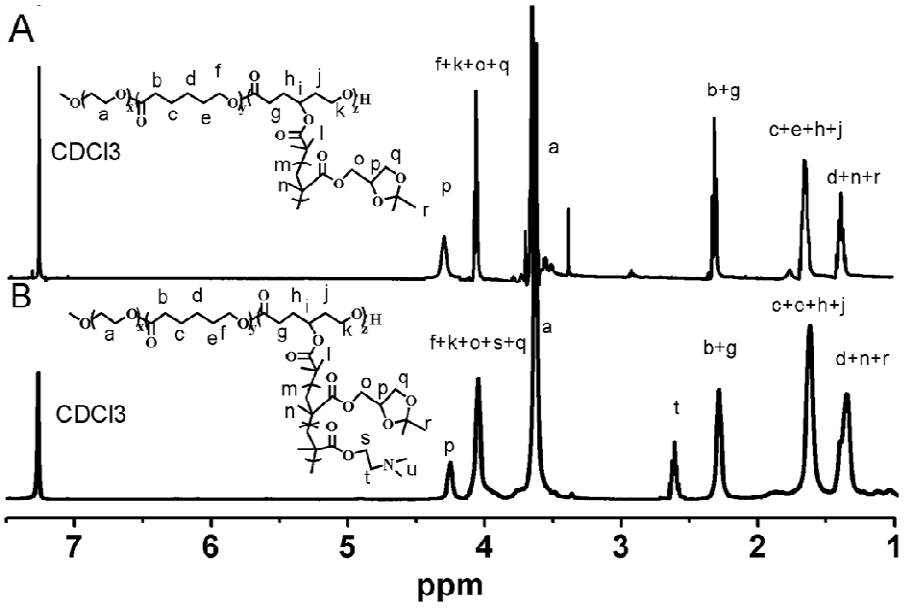

Fig. 2

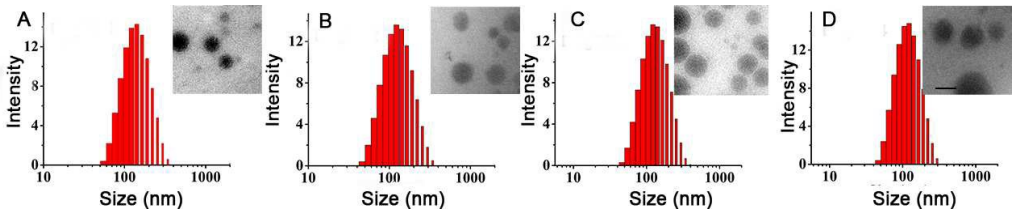

Fig. 3

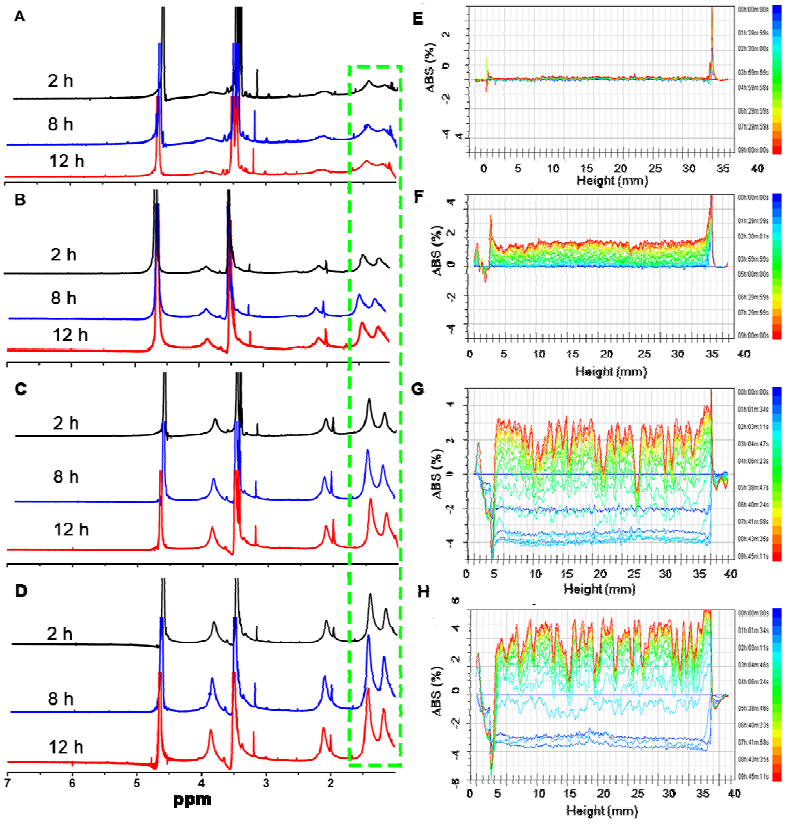

Fig. 4

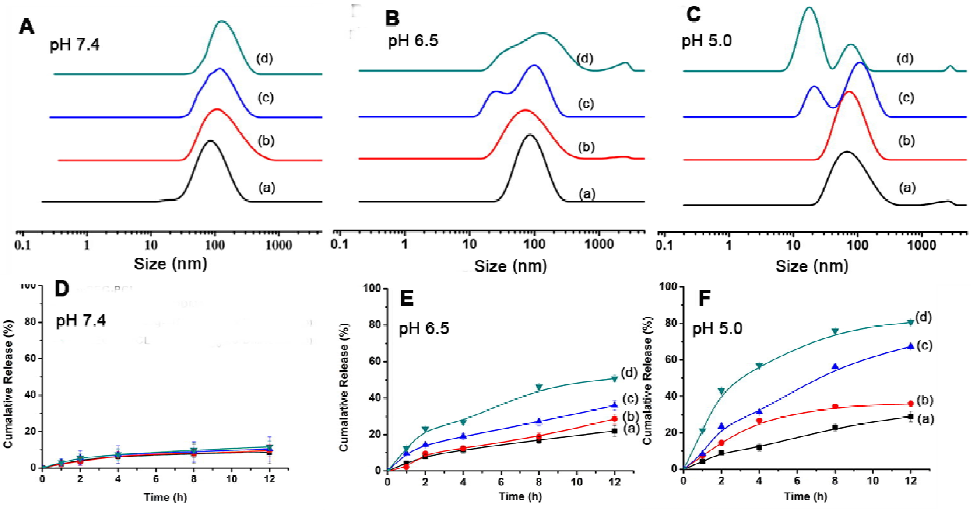

Fig. 5

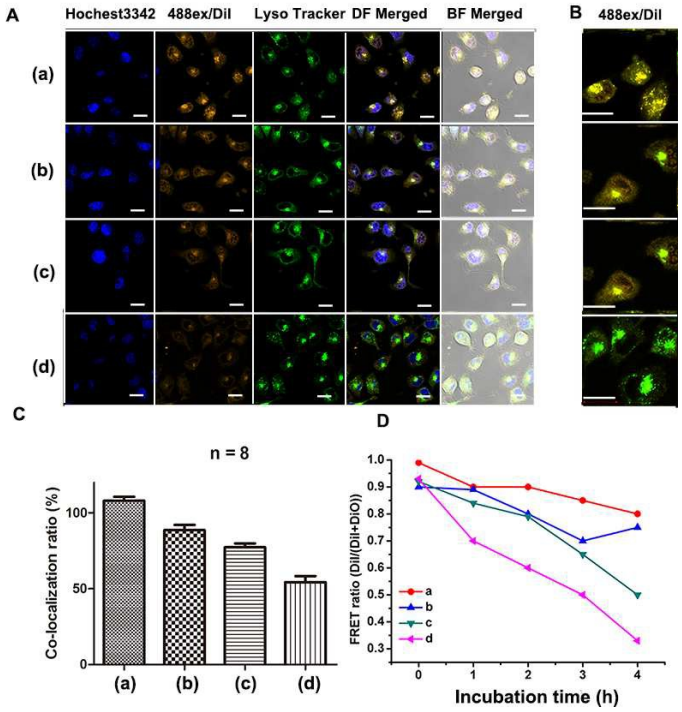

Fig. 6

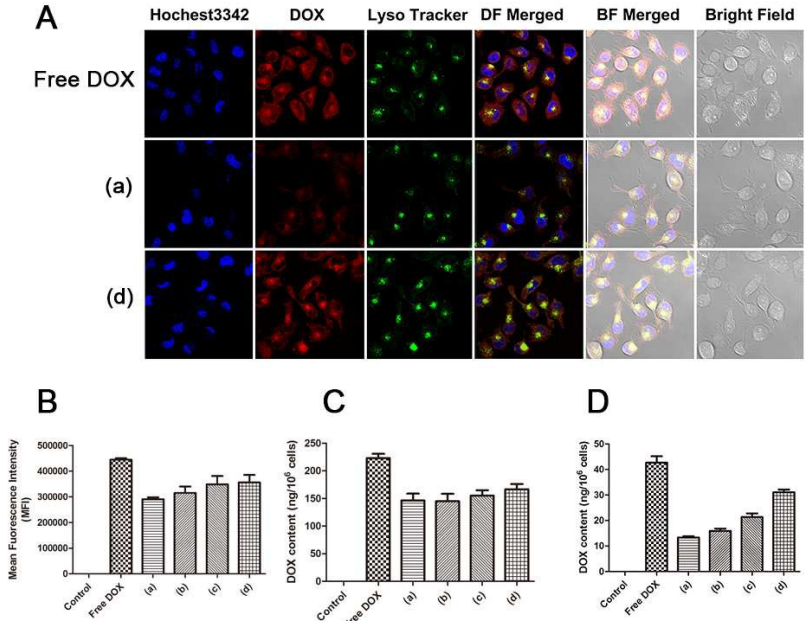

Fig. 7